Check for updates

Yuncong Feng
Department of Mechanical and Automation Engineering,
The Chinese University of Hong Kong,
G09 William M.W.Mong Engineering Building,
Shatin, Hong Kong SAR 999077, China
e-mail: ycfeng@mae.cuhk.edu.hk

Weike Zheng
Department of Mechanical and Automation Engineering,
The Chinese University of Hong Kong,
G09 William M.W.Mong Engineering Building,
Shatin, Hong Kong SAR 999077, China
e-mail: weikez@foxmail.com

Zizhao Zhao
School of Mechanical Engineering,
Northwestern Polytechnical University,
127 Youyi West Road,
Xi'an 710072, China
e-mail: zhaozizhaonwpu@163.com

Biao Liang
School of Mechanical Engineering,
Northwestern Polytechnical University,
127 Youyi West Road,
Xi'an 710072, China
e-mail: biao.liang@nwpu.edu.cn

Haitao Ye
Department of Mechanical and Energy Engineering,
Southern University of Science and Technology,
1088 Xuanyuan Avenue,
Shenzhen 518131, China
e-mail: 12069004@mail.sustech.edu.cn

Qi Ge
Department of Mechanical and Energy Engineering,
Southern University of Science and Technology,
1088 Xuanyuan Avenue,
Shenzhen 518131, China
e-mail: geq@sustech.edu.cn

Xiangyi Zhang
Shandong Jiangshan Fiber Technology Co. Ltd.,
Middle of Taoyuan Avenue,
Dezhou 253100, China
e-mail: zhangxy637@sina.com

Weizhao Zhang[1]
Department of Mechanical and Automation Engineering,
The Chinese University of Hong Kong,
RM216 William M.W.Mong Engineering Building,
Shatin, Hong Kong SAR 999077, China
e-mail: weizhaozhang@cuhk.edu.hk

Characterization and Finite Element Modeling for Thermoset Resin of Carbon Fiber Prepregs During Curing

In this study, an epoxy resin, YZ-05, designed specifically for carbon fiber reinforced polymer prepregs, was characterized and modeled. A degassing method for the highly viscous YZ-05 was established for specimen preparation. To numerically model the behavior of YZ-05 in curing, several components, including the heat transfer, curing kinetics, and viscoelastic constitutive law ones, were developed, and the corresponding material properties to be input were tested. As YZ-05 shows severe creep at high temperature under mechanical loading, the combination of digital image correlation (DIC) and thermography technique was utilized to obtain its thermal expansion and chemical shrinkage. In the aspects of viscoelastic behavior, stress relaxation tests were performed based on time–temperature superposition principle with a numerical method to calculate shift factors. After development and input identification, these modeling components for YZ-05 resin were integrated and the modeling results were validated using experiments, where bending of resin beams was induced during curing. [DOI: 10.1115/1.4053731]

Keywords: polymer fabrication processes, modeling and simulation, material handling, injection molding and other polymer fabrication processes

Downloaded from http://asmedigitalcollection.asme.org/manufacturingscience/article-pdf/144/8/081007/6846352/manu_144_8_081007.pdf by Southern University of Science & Technology user on 18 April 2022

[1]Corresponding author.
Manuscript received November 24, 2021; final manuscript received January 23, 2022; published online February 16, 2022. Assoc. Editor: Martine Dubé.

Copyright © 2022 by ASME

1 Introduction

Thermoset carbon fiber reinforced polymer (CFRP) draws great attention from both industries and academia due to its high strength-to-weight ratios, good corrosion resistance, and excellent geometric conformability [1,2]. For the mass production of CFRP products, various manufacturing methods, such as resin transfer molding (RTM), thermoforming, and pultrusion, have been established. For thermoset CFRPs, resin curing is an indispensable step in all manufacturing methods. Because of thermal expansion and chemical shrinkage, curing usually induces residual stress, causing unwanted deformation or even crack. To solve this issue and reduce residual stress, curing parameters and mold geometry need to be optimized with the assistance of process modeling [3,4]. However, modeling CFRP curing is challenging, partly because (1) properties of epoxy resin are temperature and degree of curing (DOC) dependent and (2) resin is highly viscoelastic during curing.

In this study, a prepreg-exclusive epoxy resin, YZ-05, was characterized and modeled in the aspects of curing kinetics, thermal properties, thermal and chemical strain, and viscoelasticity. Figure 1 demonstrates the modeling components involved and their relationship with each other. Accurate characterization of material properties is the foundation of successful numerical modeling. To measure curing kinetics, the isothermal scan by differential scanning calorimeter (DSC) is commonly selected to eliminate the effect of temperature [5–7]. As for thermal properties, specific heat capacity, thermal diffusivity, and mass density are usually obtained using the DSC, flash analysis method [8], and Archimedes' principle [9], respectively. Then, heat conductivity can be derived from the theoretical calculation. Thermal expansion and chemical shrinkage are conventionally obtained by the thermomechanical analysis (TMA) [10,11]. However, TMA cannot be easily applied in this study, as uneven surfaces of cured samples caused by chemical reaction and mold geometry can be hardly removed by a polish that will generate heat and change DOC of the samples. The uneven surfaces will lead to nonuniform deformation in TMA, causing measurement inaccuracy. Moreover, it has been observed that the curing reaction of YZ-05 resin happens above the glass transition temperature when serious creep can occur. Therefore, it is impossible to measure the chemical shrinkage of YZ-05 using the contact technique.

For viscoelasticity characterization, stress relaxation tests using dynamic mechanical analyzer (DMA) are mostly utilized [12,13]. Obtaining long-term stress relaxation curves using experiments is time-consuming and labor-intensive. Thus, time–temperature superposition principle (TTSP) has been established to convert short-term relaxation tests in a range of temperatures into a long-term relaxation modulus master curve using shift factors [14–16]. Although TTSP has been used and validated for various polymers previously, there is no universal approach to derive shift factors. Several authors presented automatic algorithms to implement relaxation curve shifting [17,18]; however, these methods are based on curve fitting that could introduce error from function selection. Liu et al. [19] developed a data-driven formula to determine shift factors, but this formula only works for rheological simple materials.

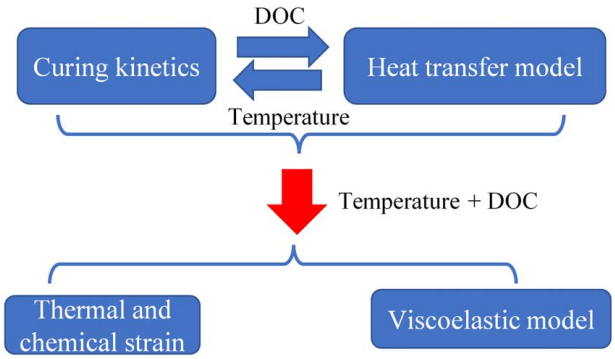

Fig. 1 Relationship among different components in curing modeling

Apart from characterization, the high viscosity of YZ-05 resin leads to difficulty in degassing during sample preparation. The vacuum method [20] is commonly used for degassing resin since bubbles become less soluble under lower air pressure. To prevent resin from precuring and even boiling, the resin is usually degassed at ambient temperature, which, however, cannot work on YZ-05 since bubbles inside would be trapped by the high viscosity of the resin at ambient temperature. To reduce viscosity and at the same time avoid precuring and boiling, a temperature stepwise vacuum method was adopted based on the DSC measurement.

To tackle the issues abovementioned in experimental characterization, in this study, the fabrication of partially/fully cured resin samples with the special degassing procedure (Sec. 2) was established. Subsequently, curing kinetics was determined using the isothermal scan of DSC, and the obtained kinetic equation is validated by isothermal scan under different conditions (Sec. 3). Afterward, thermal properties were experimentally characterized as modeling input (Sec. 4). Then, based on the technique documented in Ref. [21], digital image correlation (DIC) combined with the thermography technique was applied to measure thermal expansion and chemical shrinkage coefficients of the resin under elevated temperature (Sec. 5). Next, a data-driven method was developed to calculate the shift factors to construct the viscoelasticity master curve (Sec. 6). Finally, the obtained material properties were input to the resin curing numerical model, which was then validated using experiments where resin beam samples were cured and deformed under nonuniform temperature boundary conditions.

2 Material and Sample Preparation

Epoxy resin in this study, YZ-05, is provided by Shandong Jiangshan Fiber Technology Co., Ltd. (Dezhou, China). YZ-05 is made up of bisphenol-A 128/902 mixed with dicyandiamide 100S as a curing hardener. YZ-05 is a prepreg resin, and for ease of storage, the fully uncured YZ-05 requires a higher temperature to initiate curing compared with that of partially cured YZ-05. This curing temperature feature was utilized in resin sample degassing and will be further discussed in Sec. 4.2.

When fabricating resin samples, the first critical step is degassing. YZ-05 resin shows great viscosity at room temperature, making it impossible to be degassed by vacuum at ambient temperature. Thanks to the abovementioned high temperature resistance to precuring of fully uncured resin, this issue is tackled by putting YZ-05 in a vacuum environment under a relatively high temperature to lower the viscosity and eventually drag bubbles out. The temperature should be precisely controlled to effectively reduce resin viscosity while avoiding precuring. Based on the curing kinetic tests to be elaborated in Sec. 3, the upper limit of the degassing temperature should be 110 °C, below which the curing rate is negligible. As for the lower limit, experiments using a heat gun and an infrared (IR) camera indicated that the resin would exhibit good flowability starting from 80 °C.

Once the degassing temperature range was determined, fabrication of YZ-05 samples started with putting the resin at around 20 °C into silicone molds made from RTV664-J (Momentive, Tokyo, Japan). Subsequently, the resin was placed into the vacuum oven at 80 °C until it can flow. Next, the oven was vacuumed and heated up to 95 °C to burst bubbles. Afterward, the resin was taken out, and the top surface was swept away to eliminate leftover bubbles. Then, the resin was heated up to 105 °C to further reduce viscosity, and the top surface was swept once more to remove any possible new bubbles. Finally, the resin was cured at 110–150 °C depending on the target DOC. After curing, the DOC of the samples was determined using the isothermal scan of DSC [22]. During the scan, the temperature rose from 30 °C to 160 °C at the rate of 80 °C/min first and then held for 30 min until the samples were completely cured.

Downloaded from http://asmedigitalcollection.asme.org/manufacturingscience/article-pdf/144/8/081007/6846352/manu_144_8_081007.pdf by Southern University of Science & Technology user on 18 April 2022

Table 1 Total heat generation for different DSC measurements

	Isothermal scanning				Dynamic scanning		
DSC measurements	110 °C	120 °C	140 °C	160 °C	3 °C/min	6 °C/min	10 °C/min
Heat generation (J/g)	343	382	391	418	410	408	403

Table 2 Curing kinetic parameters of the YZ-05 resin

Parameter	Value (kJ/mol)	Parameter	Value (s^{-1})	Parameter		Value
$E_{a,1}$	125.4	A_1	2.94×10^{12}	m	($\alpha\le0.5$)	$-0.008*T+1.8239$
$E_{a,2}$	62.7	A_2	1.61×10^{6}		($\alpha>0.5$)	$-0.024*T+3.0123$
				n	($\alpha\le0.5$)	$0.0122*T+0.5119$
$E_{a,3}$	35.6	A_3	1.10×10^{2}		($\alpha>0.5$)	0.9

3 Curing Kinetic Modeling and Testing

3.1 Fundamental Theory of Curing Kinetics. Curing of thermoset polymer can be precisely captured with the assumption that curing rate is proportional to heat flow [23–25]

$$\frac{da}{dt} = (dH/dt)/\Delta H_t \tag{1}$$

where da/dt and dH/dt denote the reaction rate and heat flow, respectively. ΔH_t represents total heat generation in curing, obtained by the integral of the exothermic peak of the heat flux curve. The total heat generation was measured from isothermal conditions of 110, 120, 140, and 160 °C and dynamic scanning at 3, 6, and 10 °C/min using DSC (Q1000, TA Instrument, New Castle, DE). For isothermal measurements, the temperature initially ramped at 80 °C/min from 40 °C to the target curing temperatures of 110, 120, 140, or 160 °C. Then, the temperature was held for 80 min for temperatures of 110 or 120 °C, or 30 min for temperatures of 140 or 160 °C to complete curing. For dynamic scanning, the temperature was increased from 30 up to 250 °C with a rate of 3, 6, or 10 °C/min. The results are presented in Table 1. ΔH_t is the largest measured heat generation in experiments, which is 418 J/g from isothermal scan at 160 °C. Then, DOC can be calculated as

$$a = \frac{\Delta H(t)}{\Delta H_t} \tag{2}$$

where ΔH is the accumulated heat estimated by integrating the DSC peak up to time t.

3.2 Autocatalytic Model. Experimental results show that the autocatalytic model can capture curing kinetics of the YZ-05 resin with the highest accuracy. The autocatalytic model can be expressed as

$$\frac{da}{dt} = (k_1 + k_2\alpha^m)(1-\alpha)^n \tag{3}$$

where reaction rate constants k_i ($i=1, 2$) are calculated using the Arrhenius law

$$k_i = A_i \exp\left(-\frac{E_{a,i}}{RT}\right) \quad (i=1, 2) \tag{4}$$

where A_i are the pre-exponential factors and $E_{a,i}$ denote the activation energy. R is the universal gas constant of 8.31 J/mol · K and T refers to material temperature. With the initial conditions of $\alpha(0)$ being 0, k_1 can be obtained from Eq. (4) as

$$k_1 = \frac{da}{dt}|_{t=0} \tag{5}$$

where $da/dt|_{t=0}$ was measured from the isothermal reaction rate curves. The determination of kinetic parameters k_2, m , and n is the core of curing kinetic model development, and in this study, these parameters were determined using the Kenny analytical–graphical method combined with segmented characterization [26].

3.3 Differential Scanning Calorimeter Characterization. In this research, the curing kinetics of YZ-05 resin was characterized under isothermal scanning conditions with temperatures of 110, 120, 140, and 160 °C as described in Sec. 3.1. The sample weight before DSC testing was 2 mg, same as that in the following validation tests and residual heat measurement. Argon was used as a protective gas in all DSC measurements. Experiments under each test condition were repeated three times to calculate the average results.

The characterized autocatalytic model is established as follows:

$$\begin{cases} \dfrac{d\alpha}{dt} = (k_1 + k_2\alpha^m)(1-\alpha)^n, & \alpha \in (0, 0.5] \\ \dfrac{d\alpha}{dt} = (k_3\alpha^m)(1-\alpha)^n, & \alpha \in (0.5, 1] \end{cases} \tag{6}$$

It should be noted that k_1 is canceled out from the model when α ranges from 0.5 to 1, as k_1 implies the effect of the initial point, which is not contained in the second segmentation. After DSC measurement, the values of the parameters in Eq. (4) for k_i and exponentials m and n in Eq. (6) were determined through iteration and the results are listed in Table 2. Figure 2 shows the curing kinetic curves between the characterized model and experimental measurement.

3.4 Validation of Autocatalytic Model. Once the curing kinetic model and its input parameters were determined, the model was validated by DSC isothermal scanning at 150 °C with

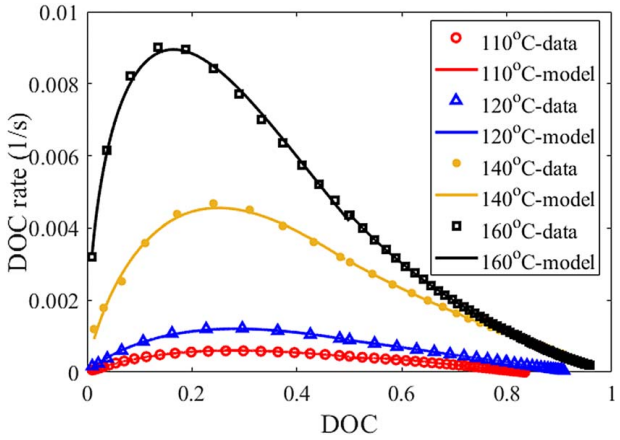

Fig. 2 Autocatalytic model fitting with experimental data

Downloaded from http://asmedigitalcollection.asme.org/manufacturingscience/article-pdf/144/8/081007/6846352/manu_144_8_081007.pdf by Southern University of Science & Technology user on 18 April 2022

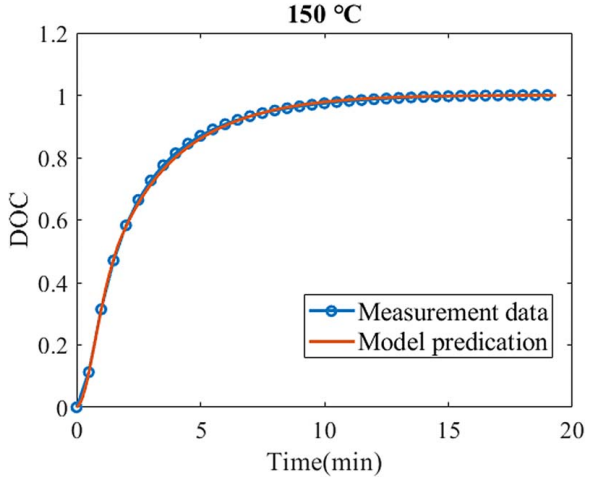

Fig. 3 Model validation with the DSC experiment using isothermal scanning at 150 °C

Table 3 Density measurement for the resin with different curing states

Sample number	Curing temperature (°C)	Curing time (min)	Density (g/cm^3)
1	110	15	1.2071
2	110	25	1.2188
3	110	30	1.2143
4	110	35	1.2159
5	110	40	1.2120

the same procedure as that of 140 and 160 °C. The comparison is shown in Fig. 3, where the time starts from the onset of curing reaction instead of the real measurement for better illustration. It can be observed that under this condition, the prediction error of the model is only 0.1%.

4 Heat Transfer Modeling and Testing

The temperature distribution within the material domain is crucial in modeling residual stress during curing as resin properties are temperature dependent. In this study, transient temperature variation within the resin during curing is modeled by the three-dimensional (3D) isotropic Fourier's law as

$$\rho C \frac{\partial T}{\partial t} = \frac{\partial}{\partial x_i}\left(k \frac{\partial T}{\partial x_i}\right) + \dot{\phi} \tag{7}$$

where ρ, C, and T represent the mass density, specific heat capacity, and temperature of the YZ-05 resin, respectively. k is the heat conduction coefficient of the resin, and x_i represents 3D spatial coordinates. $\dot{\phi}$ is the internal heat source induced by chemical reaction, and it is denoted by

$$\dot{\phi} = \rho \Delta H_t \frac{d\alpha}{dt} \tag{8}$$

Since ΔH_t and $d\alpha/dt$ have been determined in Sec. 3.3 during the characterization of curing kinetics, the remaining parameters to be identified are ρ, C, and k.

4.1 Mass Density. The mass density was measured following ASTM D792 [27]. Samples with different curing states were tested and presented in Table 3. As no obvious tendency of density variation is observed when the curing state changes, the resin is assumed to have a constant average density of 1.214 g/cm^3 during curing.

4.2 Specific Heat Capacity. The DSC was applied to characterize the specific heat capacity of the YZ-05 resin in accordance with ASTM E1269-11 [28]. Resin with an average weight of 2 mg and different DOCs of 0, 0.28, 0.41, 0.74, and 1 were tested to investigate the relationship between DOC and specific heat capacity. All tests were conducted from 20 °C to 150 °C at the rate of 10 °C/min to cover the real curing temperature range. Testing on each DOC group was repeated three times, and the average results are shown in Fig. 4(*a*). The result of samples with 0.74 DOC is taken as an example to demonstrate specific heat capacity variation under elevated temperature, as shown in Fig. 4(*b*).

Curing reaction starts from the peak of specific heat capacity curve as shown in Fig. 4(*b*), which will be elaborated on later in this paragraph. As observed from Fig. 4(*a*), the temperature corresponding to the peak of specific heat capacity curve for YZ-05 resin with 0 DOC is around 112 °C, significantly higher than those of partially cured samples, indicating that the uncured YZ-05 resin requires the higher initial temperature to start curing, although once curing has been initialized, the onset temperature of curing displays positive relation with DOC as normal resins do [21,29,30]. The reason for this high temperature resistance of YZ-05 with 0 DOC is that this resin is designed specifically as a prepreg matrix, and for ease of storage, stabilizer constituents have been added to prevent it from precuring at low temperature.

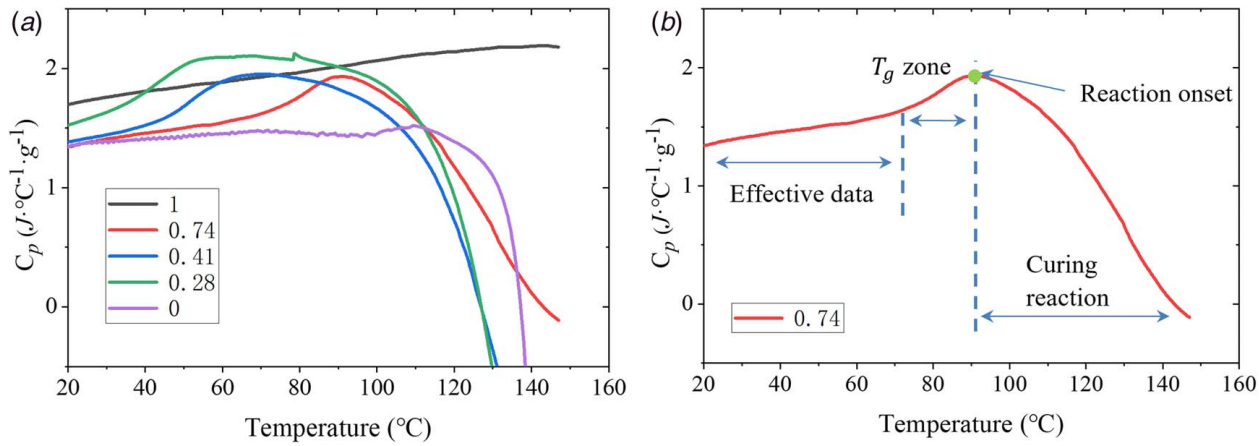

Fig. 4 Average specific heat capacity for samples with (*a*) different DOCs and (*b*) the DOC of 0.74 as a representative under elevated temperatures

Downloaded from http://asmedigitalcollection.asme.org/manufacturingscience/article-pdf/144/8/081007/6846352/manu_144_8_081007.pdf by Southern University of Science & Technology user on 18 April 2022

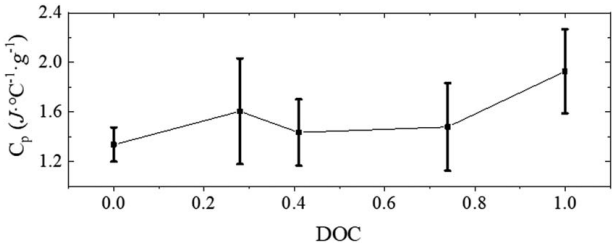

Fig. 5 Average specific heat capacity versus different DOCs

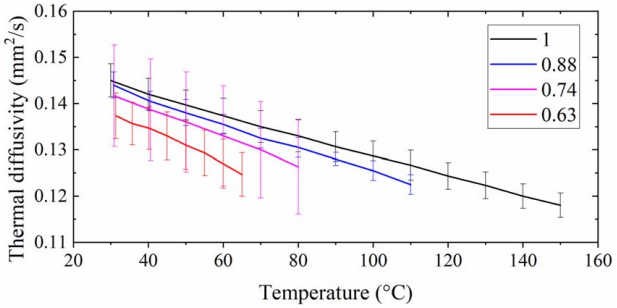

Fig. 6 Thermal diffusivity of resin with different DOCs under elevated temperatures

However, after curing initialization, these stabilizer constituents will decompose, making curing happen at a lower temperature. Figure 4(*b*) shows that specific heat capacity grows mildly as temperature increases until the glass–rubber transition (T_g) zone, where the specific heat capacity curve turns to a sharp increase. Afterward, the heat-releasing curing begins, so the heat absorption changes to heat-releasing until the end of the measurement. Since curing mainly happens above T_g, specific heat capacity should be calculated using data measured below this temperature point. Following this criterion, the average specific heat capacity of samples with various DOCs was obtained and is demonstrated in Fig. 5. As no obvious trend can be observed when the testing deviation is considered, it is assumed that the YZ-05 resin has DOC-independent specific heat capacity of 1.564 J/(g ·°C).

4.3 Thermal Conductivity. Thermal conductivity is the product of mass density, specific heat capacity, and thermal diffusivity, the former two of which have been measured in Secs. 4.1 and 4.2. Thermal diffusivity was determined using Light Flash Apparatus (LFA 467, NETZSH) following ASTM E1461-13 [31]. The dimension of the specimens was ø12.7 × 1 mm. Samples with DOCs of 0.63, 0.74, 0.88, and 1 were measured from 30 °C to T_g, because glass transition would not only change specimen DOC but also significantly affect heat transfer due to enthalpy change. The measurement was conducted with a laser pulse width of 300 μs and voltage of 250 V, and nitrogen as protective gas. Experiments for each DOC group were repeated three times, and the results are shown in Fig. 6.

Although thermal diffusivity shows variation when sample DOC or temperature changes, the variation does not exceed the maximum testing deviation. Therefore, for modeling convenience, thermal diffusivity was considered as DOC- and temperature-independent, with the average value of 0.139 mm^2/s. Then, the thermal conductivity of YZ-05 resin was calculated as 0.264 W/(m ·°C).

5 Viscoelastic Modeling and Testing

The viscoelastic constitutive equation for resin relaxation can be expressed as [32,33]

$$\boldsymbol{\sigma}_i = \boldsymbol{C}_{ij}^{\infty}\boldsymbol{\varepsilon}_j^{\text{eff}}(t) + \sum_{m=1}^{N}\boldsymbol{C}_{ij,m}\boldsymbol{q}_{j,m}(t), \quad i,\ j = 1 \text{ to } 6 \tag{9}$$

where

$$\boldsymbol{q}_{j,m}(t) = \exp\left(-\frac{\Delta\xi_t}{\tau_m(\alpha_t)}\right)\boldsymbol{q}_{j,m}(t-\Delta t) + \frac{1-\exp\left(-\dfrac{\Delta\xi_t}{\tau_m(\alpha_t)}\right)}{\Delta\xi_t/\tau_m(\alpha_t)}\Delta\boldsymbol{\varepsilon}_j^{\text{eff}}(t) \tag{10}$$

where $\Delta\xi_t = \int_{t-\Delta t}^{t}(1/a_T(\alpha, T))ds$, and $a_T(\alpha, T)$ is the shift factor. τ_m represents discrete relaxation time. Subscript t indicates that the quantity is in current time t. $\Delta\boldsymbol{\varepsilon}_j^{\text{eff}}(t)$ is the increment in current time-step Δt of the effective strain, which is defined as

$$\boldsymbol{\varepsilon}_j^{\text{eff}} = \boldsymbol{\varepsilon}_j - \text{CTE}_j \cdot \Delta T - \eta_j \cdot \Delta\alpha \tag{11}$$

where $\boldsymbol{\varepsilon}_j$ is the total strain; CTE_j and η_j are thermal expansion coefficients (CTE) and chemical shrinkage coefficients (CSC), respectively.

In this study, CTE and CSC of the YZ-05 resin were characterized using DIC coupled with an IR camera. $\boldsymbol{C}_{ij}^{\infty}$, $\boldsymbol{C}_{ij,m}$, τ_m, and a_T, on the other hand, were measured with stress relaxation experiments on DMA 850 (TA Instruments).

5.1 Function Between Glass Transition Temperature and Degree of Curing. Prior to the identification of material properties in Eqs. (9)–(11), sample DOC needs to be measured as the mechanical performance of resin will be significantly influenced by its cross-linking status. However, the DOC of partially cured samples used in CTE and CSC measurement, as well as the subsequent verification experiments, can hardly be determined by DSC because (1) DOC distribution within large samples is not uniform due to heat transfer and exothermic reaction during fabrication, so taking a crushed part out of a large sample for DSC measurement cannot represent the whole piece, and (2) samples in these experiments must remain intact, so they cannot be tested by DSC beforehand. As an alternative, the average DOC of samples in viscoelasticity characterization and verification will be indirectly measured using T_g.

The relationship between T_g and DOC of the YZ-05 resin was identified by DMA 7e (Perkin Elmer, Waltham, MA) following ASTM D7028-07 [34]. During tests, the three-point bending mode was adopted and the sample dimension was 5 × 25 × 1 mm (width × length × thickness). The length of samples was larger than the 20 mm width of the sample holder, and the excessive part was cut off for DSC measurement to determine sample DOC. Due to a small thickness, curing was regarded as uniform across the sample. A 1-Hz cycled loading was added to the beam samples under a heating rate of 5 °C/min from 25 °C to 150 °C, and the temperature at the peak of the loss modulus is T_g. Tests for each DOC group were repeated three times.

The average T_g of the YZ-05 resin with various DOCs is shown in Fig. 7. Using the second-order polynomial regression, the

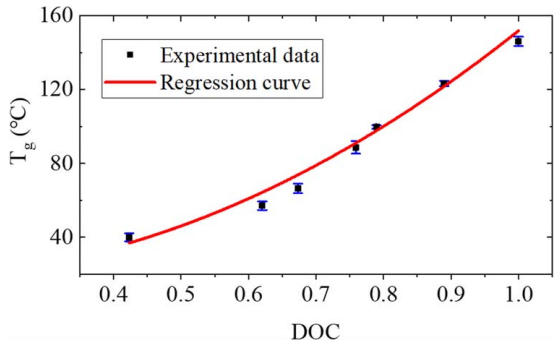

Fig. 7 T_g of the YZ-05 resin with various DOCs

Downloaded from http://asmedigitalcollection.asme.org/manufacturingscience/article-pdf/144/8/081007/6846352/manu_144_8_081007.pdf by Southern University of Science & Technology user on 18 April 2022

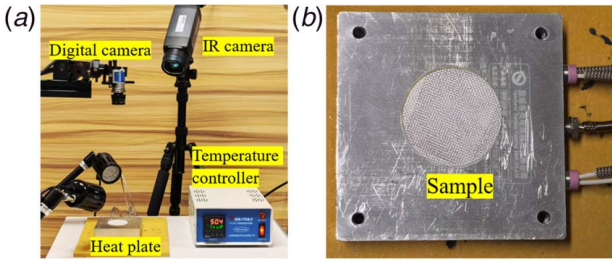

Fig. 8 (*a*) Thermal expansion and chemical shrinkage measurement setup and (*b*) speckle pattern on the sample

relationship between T_g and DOC can be expressed as

$$T_g(\alpha) = 19.46 - 25.73\alpha + 158.14\alpha^2 \tag{12}$$

This function is also shown in Fig. 7 for comparison. It should be noted that Eq. (12) was derived using samples with DOC over 0.40, as samples with less than 0.40 DOC behave more like a fluid than solid and can only store negligible residual stress.

5.2 Thermal Expansion and Chemical Shrinkage Coefficients. CTE and CSC of polymer are commonly measured using TMA [10,11]. However, this method does not work for the YZ-05 resin. First, the curing reaction of YZ-05 would be initialized only after phase transition when severe creep would happen, so chemical shrinkage cannot be distinguished from the creep in the contact mode measurement. Second, the geometry quality of the samples imposes a significant impact on TMA accuracy. In preparation of partially cured samples, only limited polishing could be applied to avoid excessive heat generation that can cause further curing. This might lead to uneven and unparallel top and bottom sample surfaces, resulting in nonuniform pressure and displacement at the sample–TMA interface. These uncontrollable variables in partially cured samples make a measurement using TMA difficult. As a solution, in this study, a noncontact method combining DIC and thermography technology was developed based on the work in Ref. [21] to measure CTE and CSC of the YZ-05 resin samples.

The setup of the system for noncontact measurement is shown in Fig. 8(*a*), and it consists of a 12MP camera equipped with a 28-mm lens (Schneider), a heat plate (Germay Heater) connected with a temperature controller, and an IR camera (FLIR) to record temperature on the top surface of the sample during curing. The software VIC-2D (Correlation Solutions, Irmo, SC) was used to calculate the planar strain of the sample. The sample was stamped with a speckle pattern after its top surface was sprayed with acrylic resin paint for DIC tracking, as shown in Fig. 8(*b*). Temperature measurement using thermography technique depends on the surface emissivity of the sample, and the acrylic paint has an emissivity coefficient of 0.94. The digital camera was placed orthogonal to the sample for accurate in-plane deformation recording, and its height was adjusted until the full speckle pattern on the sample was captured in the field of view. The heat plate was sprayed with demoulding agent to reduce friction and adhesion at the resin–plate interface. The sample with a size of ϕ 46 mm × 1 mm was prepared with different DOCs following the procedures in Sec. 2. The temperature started from 25 °C to 150 °C at the rate of 10 °C/min and followed by temperature dwelling for 30 min until the curing completed.

For data analysis after measurement, the top surface of the sample was selected as the region of interest (ROI). In Fig. 9(*a*), *y*-axis represents the temperature difference along pixels of ROI at the same horizontal position. It can be observed that the maximum temperature variation is less than 2.5 °C when the average temperature of ROI is 137.5 °C. Therefore, the temperature distribution can be

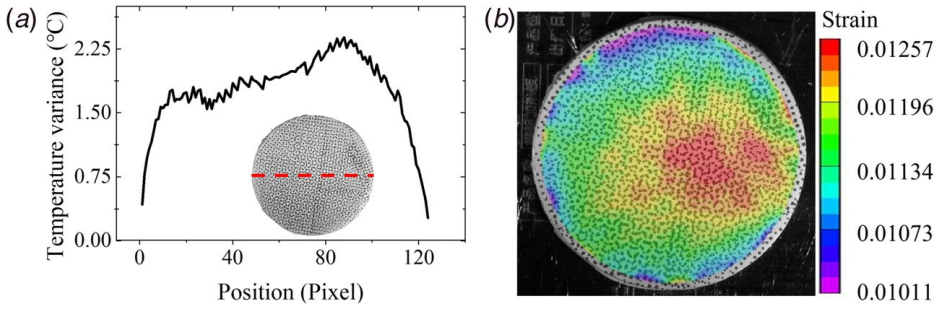

Fig. 9 (*a*) Tempreature variation on the sample surface along the horizontal line marked by the dash line and (*b*) thermal strain distribution on the YZ-05 sample in the heating step at 92 °C captured by the DIC

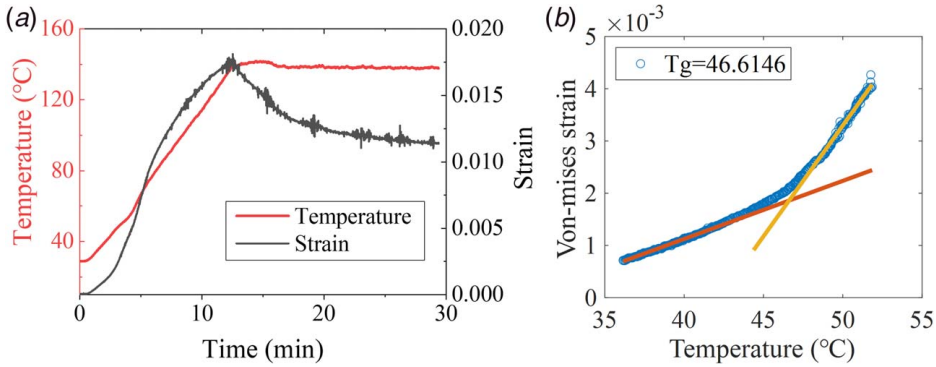

Fig. 10 (*a*) Temperature history and strain growth of one sample during the test and (*b*) T_g determined from the temperature curve

Downloaded from http://asmedigitalcollection.asme.org/manufacturingscience/article-pdf/144/8/081007/6846352/manu_144_8_081007.pdf by Southern University of Science & Technology user on 18 April 2022

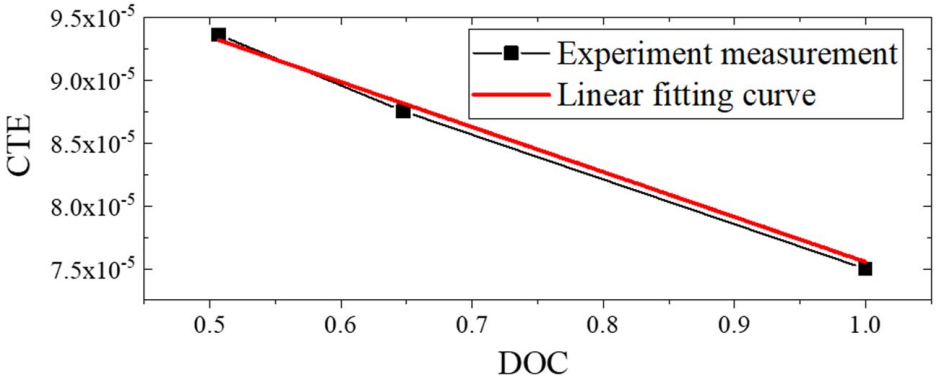

Fig. 11 CTE versus DOC of the YZ-05 resin

considered uniform. Although not affecting the measurement of resin temperature, it should be noted that the emissivity of aluminum deviates significantly from that of the white acrylic paint, so the temperature read of the heat plate is inaccurate. One example of the thermal strain distribution at 92 °C captured by DIC is shown in Fig. 9(*b*). Since polymer resin is isotropic in CTE and CSC, the average strain value from DIC will be utilized for the subsequent analysis.

Figure 10(*a*) demonstrates the temperature history captured by the IR camera and the true strain development induced by thermal expansion and chemical shrinkage. Variation in the slope of the temperature curve indicates glass transition that causes an increase in specific heat capacity. The glass transition temperature is obtained by the intersection of extrapolation of the slopes of pre- and post-transition regions according to ASTM E1545-11 [35], as shown in Fig. 10(*b*). It was noticed from experiments that the difference in T_g measured by DMA and the rheological method is within 5% for the YZ-05 resin. After T_g is determined, the DOC of the sample can be derived using Eq. (12). CTE is obtained by the linear regression of the strain–temperature curve in Fig. 10(*b*) prior to T_g to avoid possible DOC variation, as well as material softening and residual stress accumulation, which will be elaborated in Sec. 5.3.

Measured CTEs of the resin with different DOCs are shown in Fig. 11. It can be observed that CTE decreases linearly as DOC increases, which has also been observed for other epoxy resins [21,36]. The regression line for CTE and DOC is

$$\text{CTE} = -3.58 \times 10^{-5}\alpha + 1.11 \times 10^{-4} \tag{13}$$

During the experiment, the DOC of the samples is difficult to be measured directly. Therefore, to correlate chemical shrinkage with DOC and obtain CSC, DOC evolution in the experiment was computed using the developed curing kinetic equations, i.e., Eq. (6), with the temperature captured by the IR camera. To eliminate the effect of thermal expansion, only shrinkage in the temperature dwelling step was taken for CSC characterization. The relationship between chemical shrinkage and DOC for different samples is shown in Fig. 12. It can be found that chemical shrinkage has a strong linear relationship with DOC, and the average value of the measured CSC is 0.02115, which will be input to the final numerical model for resin curing prediction.

The negative correlation between CTE and DOC combined with the fact that CTE grows larger after T_g explains why chemical shrinkage can hardly be observed in density measurement documented in Sec. 4.1. The samples underwent the curing cycle in material preparation, where DOC in the heating step is smaller than that in the cooling step. From Eq. (13), this DOC difference results in higher thermal expansion in heating than contraction in cooling. Moreover, this expansion-larger-than-shrinkage phenomenon was more obvious after T_g, possibly counteracting the sample volume reduction caused by chemical shrinkage.

5.3 Stress Relaxation Tests. Resin samples with the DOC of 0.41,0.50, 0.65, 0.74, 0.89, and 1 were prepared in the same dimension as that of samples in Sec. 5.1 for stress relaxation tests. Tensile load type and stress relaxation mode of DMA 850 were chosen to measure the relationship between elastic modulus and time under various temperatures. In the beginning, the sample was soaked for 3 min at the testing temperature and then deformed for 10–15 min depending on the curing states. Afterward, the sample was recovered for 3 min prior to temperature rise to the next step. The temperature increase step was set as 5 °C for samples with a lower DOC of 0.41–0.74, and 10 °C for samples with a higher DOC. These procedures were repeated from 30 °C to corresponding T_g

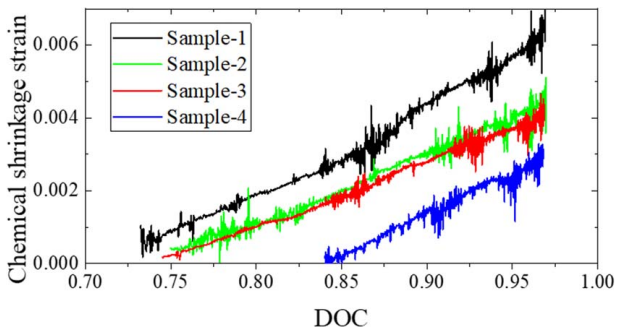

Fig. 12 Determination of the CSC of different samples

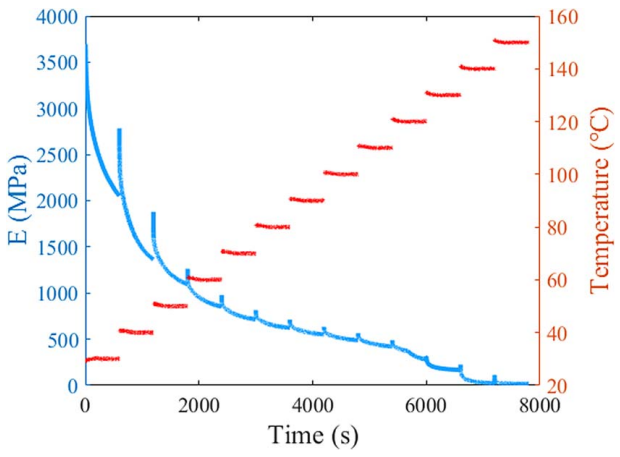

Fig. 13 Raw data of the DMA test for one sample with the DOC of 1

Downloaded from http://asmedigitalcollection.asme.org/manufacturingscience/article-pdf/144/8/081007/6846352/manu_144_8_081007.pdf by Southern University of Science & Technology user on 18 April 2022

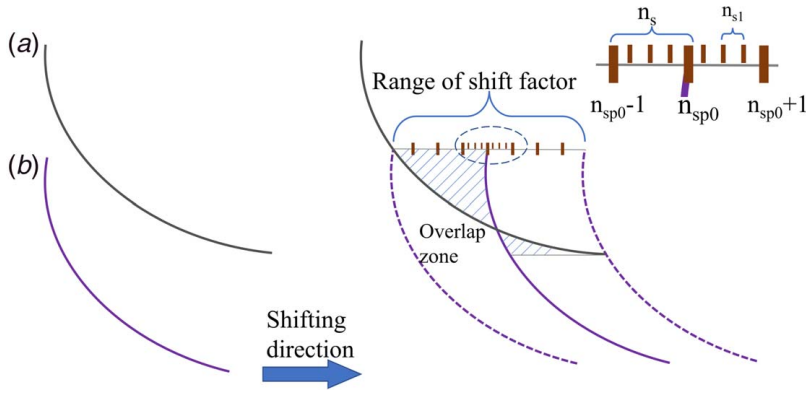

Fig. 14 In this specific shifting operation, $n_s = 8$, $n_{sp0} = 4$, and $n_{s1} = 4$

to prevent curing initiation. It should be noted that samples with the DOC of 0.74 were used for validation, while the other samples were for characterization.

Stress relaxation data captured by DMA 850 for one sample with the DOC of 1 are shown in Fig. 13 as an example. The testing time will be converted to logarithmic form with the base of 10 for data shift and master curve construction using TTSP. T_g of fully cured samples is 146 °C, as shown in Fig. 13. Elastic modulus, E, of the fully cured samples at 150 °C decreases to nearly zero in Fig. 13, meaning that the resin becomes fully soft above T_g. This phenomenon applies to partially cured samples as well, which helps explain why thermal expansion and chemical shrinkage of the resin cannot be measured accurately using TMA above T_g.

In TTSP, to move relaxation modulus curves of different temperatures to corresponding positions, researchers have come up with different strategies. Buttlar et al. [17] determined shift factors by minimizing the horizontal distance of the overlapping portions between two adjacent curves. Naya et al. [18] proposed to shift the curves based on their first derivatives. However, these numerical methods involve regression, introducing uncertainty caused by the selection of functions. As an improvement, Liu et al. [19] presented a calculation formula of the shift factor based on experimental data. However, this formula can only work for rheological simple material. In this study, the shift factors were calculated by minimizing the overlapping area encompassed by two adjacent relaxation curves using experimental data only. The schematic of the shifting process is provided in Fig. 14. Two example curves, a and b, represent relaxation modulus curves at lower and higher temperatures, respectively. The range of the shift factors is defined as the distance between the point where b joins a and the point where b leaves a. Curve b was moved along the shift factor range in n_s equally spaced steps, and the overlap area, shown in Fig. 14, was calculated using discrete integration for each step. As a result, the smallest area can be located, denoted as n_{sp0}. Then, the subrange from $n_{sp0} - 1$ to $n_{sp0} + 1$ was discretized into n_{s1} equal steps and procedures above were repeated to pinpoint the minimum overlap area.

To fit the master curve, the Prony series model has been widely adopted because it can capture the relaxation behavior of epoxy resin on long-timescale [30,37]. To investigate the curing state effect on the terms in the Prony series, different reference times for varying curing states are usually required so that the master curve could be aligned for comparison [37]. In this study, however, the initial relaxation time τ_0 remains constant at $10^{-0.9}$ s for various curing states, so it was taken as the fixed reference time. Then, discrete relaxation time in Eq. (10) could be expressed using initial relaxation time for each DOC as

$$\tau_m(\alpha) = \tau_0 \cdot q(a) \cdot 10^m \tag{14}$$

where m ranges from 1 to 50, and $q(a)$ is one coefficient to be fitted as a function of DOC α. A challenge to use the Prony series is that a large number of coefficients need to be utilized, consuming computation resources in numerical analysis and increasing the difficulty in regression [38]. To tackle this issue, in this study, the number of terms in the Prony series was reduced based on experimental observation. Terms in the Prony series whose discrete relaxation time deviates further from peak relaxation time contribute less to the master curve. Therefore, the closer the terms are to the peak relaxation time of 10^2 s, the denser the terms of discrete relaxation time were set. After adjustment, it was determined that m should take the values of 0–11, 13, 15, 18, 22, 26, 30, 35, 40, 45, and 50.

Preliminary regression showed that for the YZ-05 resin, discrete relaxation modulus becomes constant when the exponential of discrete relaxation time is over 15. Therefore, elastic modulus for stress relaxation in the Prony series model is written as

$$\begin{aligned} E(\xi) = p_{16}(\alpha) &+ \sum_{m=0}^{N_1} p_{m+1}(\alpha) \exp\left(-\frac{\xi}{p_{15}(\alpha) \cdot 10^m}\right) \\ &+ p_{13}(\alpha) \exp\left(-\frac{\xi}{p_{15}(\alpha) \cdot 10^{13}}\right) \\ &+ p_{14}(\alpha) \sum_{m=15}^{N_2} \exp\left(-\frac{\xi}{p_{15}(\alpha) \cdot 10^m}\right) \end{aligned} \tag{15}$$

where N_1 takes the values of 0–11, and N_2 takes the values of 15, 18, 22, 26, 30, 35, 40, 45, and 50. It should be noted that $p_{15}(\alpha)$ is the $q(\alpha)$ in Eq. (14). To minimize the effect of local optimization, a genetic algorithm (GA) in MATLAB was chosen to determine all $p_{1\sim16}(\alpha)$, and the seed population was set to be 500. Constraints on $p_{1\sim16}(\alpha)$ include (1) the discrete relaxation moduli, $p_{1\sim12}$ and p_{14}, should always be non-negative and (2) when ξ exceeds the full relaxation time, the corresponding discrete relaxation terms will vanish. T_g is assumed to share the same mechanism with that of stress relaxation [30], so the exponential of full relaxation time for the resin when DOC changes can be constrained using the normalized Eq. (12) as

$$\tau(\alpha) = T_g(\alpha)/T_g(1) \cdot \tau_{\max}(1) = 6.15 - 8.135\alpha + 49.98\alpha^2 \tag{16}$$

Table 4 Linear regression term values for the suitable Prony series

p	k	b	p	k	b
1	−283.20	512.90	9	0	153.99
2	−278.77	487.59	10	167.85	−6.53
3	−265.90	555.09	13	484.53	−161.85
4	−450.81	823.08	14	−289.08	368.71
5	−236.81	472.78	15	0	1.50
6	−199.73	356.54	16	236.11	−98.01
7	−195.74	278.77	—	—	—

Downloaded from http://asmedigitalcollection.asme.org/manufacturingscience/article-pdf/144/8/081007/6846352/manu_144_8_081007.pdf by Southern University of Science & Technology user on 18 April 2022

Table 5 Polynomial regression term values for the suitable Prony series

p	A	B	C
8	−1025.18	1490.66	−335.48
11	−723.23	979.60	−207.30
12	−728.39	977.60	−202.30

where τ_{max} is the order of magnitude of full relaxation time and $\tau_{max}(1)$ is 48. Based on trends of the measured data, Prony series coefficients $p_{1\sim16}(\alpha)$ as functions of DOC α were determined using the linear regression for terms 1–7, 9–10, and 13–16, and the second-order polynomial regression for the other terms. The obtained linear functions are listed in Table 4, where $E = k\alpha + b$, and the polynomial functions are presented in Table 5, where $E = A\alpha^2 + B\alpha + C$.

The obtained master curves and the experiment results for the YZ-05 resin with various DOCs are shown in Fig. 15 for comparison. It can be observed that the developed regression method is capable of capturing resin viscoelasticity during curing.

The shift factors to construct master curves for the YZ-05 resin with different DOCs are shown in Fig. 16. It can be observed that the shift factors decrease linearly as the temperature becomes higher. In addition, the slope of the shift factor shows that the temperature function decreases as DOC increases. Therefore, the relationship among shift factors, temperature, and DOC can be described using a second-order polynomial function

$$\log(aT(\alpha, T)) = (0.296\alpha^2 + 0.775\alpha - 0.922) \times (T - T_r) \quad (17)$$

where $T_r = 30$ °C.

To construct the relaxation stiffness matrix of the resin, Poisson's ratio ν also needs to be identified. To this end, uniaxial tension tests were performed on resin samples with DOC ranging from 0.88 to 1 following ASTM D638 [39], and the deformation was captured by the DIC system. The measured Poisson's ratios with different DOCs are presented in Table 6. It has been found that the variation of Poisson's ratio during curing has a negligible impact on residual stress accumulation [30,37,40]. Therefore, in this study, Poisson's ratio of the YZ-05 resin is regarded as constant 0.4 during curing for modeling convenience.

6 Experimental Validation

Experiments were conducted to validate the established numerical model in the aspect of deformation during resin curing. Input material properties to the model were characterized as mentioned from Secs. 3 to 5. Resin with DOC lower than the gel point changes to viscous liquid during curing, and the residual stress accumulated under this condition is negligible. Therefore, the experiments were for partially cured samples with DOC over the gel point. Considering the relaxation behavior of the resin in different curing states, the initial DOC of the samples should be not lower than 0.5. The actual initial DOC of each sample was determined using Eq. (12), and T_g was identified from the strain–temperature curve measured using the DIC and IR camera, as mentioned in Sec. 5.2.

The initial dimension of the samples is shown in Fig. 17. The length and width were controlled by the mold. However, the top surface of the samples cannot be completely flat due to resin flow. As samples were partially cured, the complete polish cannot be applied, either. Therefore, to accurately capture the sample geometry, the thickness was measured every 1 cm along the length direction, as shown in Fig. 17 in the dots.

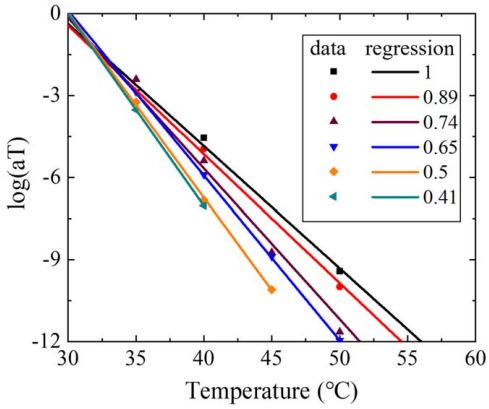

Fig. 16 Shift factors for the resin with various DOCs

Table 6 Poisson's ratios from tensile tests for resin samples with different DOCs

DOC	υ
0.88	0.372 ± 0.0058
0.92	0.40 ± 0.0312
1	0.40 ± 0.020

6.1 Experiment Setup. As shown in Fig. 18, the experiment setup consists of an IR camera to record sample temperature, a heat plate, a heat dissipator to cool down the sample, and a DIC system equipped with a 50 mm lens to capture the deformation of the sample. VIC-3D software (Correlation Solutions) was used to post-process the DIC images to measure the vertical deflection of the whole sample.

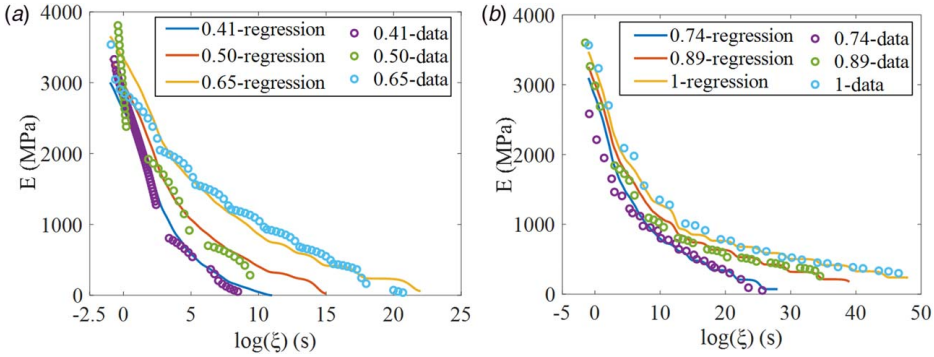

Fig. 15 Shifted stress relaxation data from experiments and master curves from regression for the resin with DOCs of (*a*) 0.41, 0.5, and 0.65; (*b*) 0.74, 0.89, and 1

Downloaded from http://asmedigitalcollection.asme.org/manufacturingscience/article-pdf/144/8/081007/6846352/manu_144_8_081007.pdf by Southern University of Science & Technology user on 18 April 2022

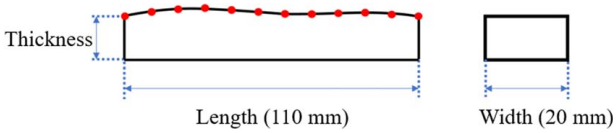

Fig. 17 Initial dimensions of the resin samples for validation experiments and the dots represent thickness measurement points

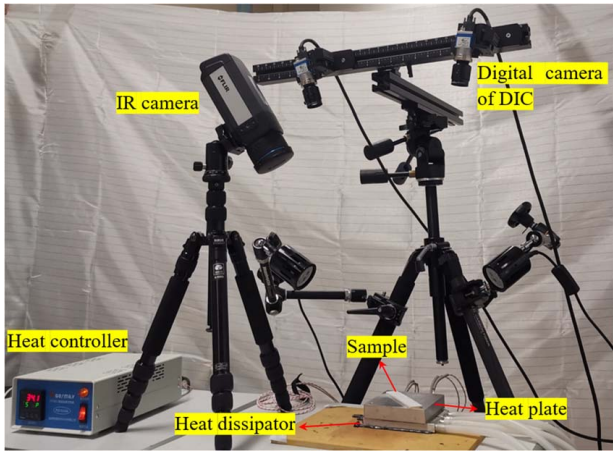

Fig. 18 Setup for validation experiments

6.2 Curing Procedures. At the beginning of curing, one sample with a speckle pattern was placed on the heat plate. Then, the temperature of the heat plate ramped from 25 °C to 160 °C in 15 min. Subsequently, the temperature holds for 30 min to fully cure the sample. Finally, the sample was cooled down by the heat dissipator to 25 °C in 4.5 min.

6.3 Simulation Configuration. Curing of the resin sample was simulated using the coupled temperature and the displacement analysis provided by the Abaqus Standard solver. The automatic time increment was used with a minimal increment of 0.01 s and a maximum at 20 s. The curing kinetic model described in Eq. (6) and the viscoelastic constitutive law described in Eqs. (9)–(10) and (15)–(17) were realized using the user subroutine UMAT. A user subroutine UEXPAN was utilized to capture DOC- and temperature-dependent thermal strain and chemical shrinkage following Eq. (11). Heat generation induced by curing reaction, as described in Eq. (8), was modeled using the user subroutine HETVAL. Heat loss due to heat convection with and radiation to the environment was considered using the user subroutine DFLUX. The measured density, specific heat capacity, thermal conductivity, and Poisson's ratio in Secs. 4 and 5.3 were input into Abaqus as essential material properties. To accurately model the sample geometry, thickness measured at different positions was utilized to create the top surface points, which were then connected by a spline curve. Afterward, the samples geometry model was discretized using 7250 C3D8T elements, as shown in Fig. 19.

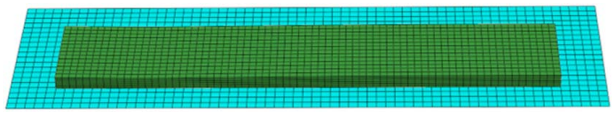

Fig. 19 Mesh of the finite element model for the validation test

To avoid the complex heat transfer modeling at the interface between the sample and the heat plate, the temperature boundary condition was applied directly to the bottom surface of the sample. The nonuniform temperature field of the sample was recorded by the IR camera, as shown in Fig. 20(*a*). As the IR camera could not see the whole bottom surface, the temperature on the bottom line of the side surface was measured, and it was assumed that temperature was constant along the sample width due to its relatively small size. In the curing cycle, because of the exothermic reaction, along the sample length direction, the temperature in the central area was higher than that of the side ones. To capture this phenomenon, the bottom line was divided into three segments with equal length, as shown in Fig. 20(*a*). Average temperature profiles of the side and middle segments of one sample during the experiment are shown in Fig. 20(*b*) as an example. It can be observed that the temperature in the middle is higher than that on the side during most of the curing time.

To apply the nonuniform temperature distribution boundary condition in simulation, the modeled bottom surface was divided into three corresponding sets, as shown in Fig. 21. The average temperature profiles of both side and middle segments measured in experiments were input directly to the side and middle sets. The two ends of the modeled bottom surface were constrained to move only in the x–z plane. The symmetry condition about the y–z plane was applied to the middle of the sample to avoid possible translational movement. In addition, the top surface of the real sample was subjected to heat dissipation to ambience through convection and radiation. To capture this heat loss, the surface heat flux was applied to the modeled top surface. The radiation was counted as a part of convection, and the heat convection coefficient was optimized to be 9.5 $W/(m^2 \cdot °C)$, so that the top temperature could be closed to the measured value. A discrete rigid plane shown in Fig. 19 was fixed and placed underneath the sample to simulate the heat plate in experiments.

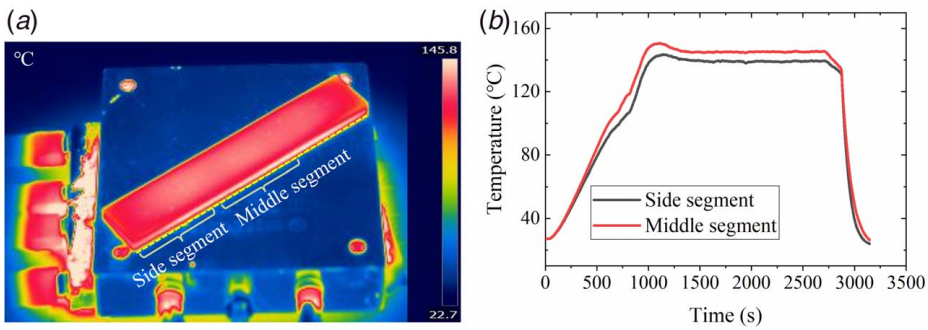

Fig. 20 (*a*) Temperature distribution of one sample in the temperature dwelling step during the validation experiment; temperature of the bottom surface was measured along the dash line and (*b*) average temperature profiles of the side and middle segments

Downloaded from http://asmedigitalcollection.asme.org/manufacturingscience/article-pdf/144/8/081007/6846352/manu_144_8_081007.pdf by Southern University of Science & Technology user on 18 April 2022

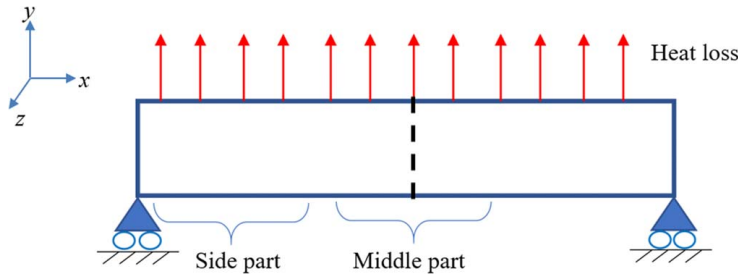

Fig. 21 Boundary conditions applied to the sample in simulation

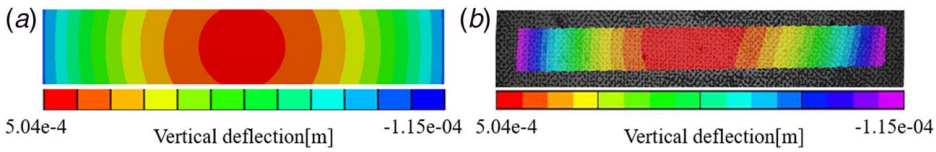

Fig. 22 Post-curing deflection on the top surface of one sample from the (*a*) simulation and (*b*) experiment

Table 7 Comparison of deflection and DOC between experiments and simulation

Sample number	Thickness (mm)	Initial DOC	Final DOC in experiments	Final DOC in simulation	Measured deflection (mm)	Predicted deflection (mm)	Error (%)
1	2.97 ± 0.17	0.65	1.00	0.97	0.640	0.665	3.8
2	2.71 ± 0.12	0.75	0.98	0.95	0.370	0.415	10.8
3	2.84 ± 0.25	0.77	1.00	0.96	0.504	0.474	6.3

Note: The final DOCs from both experiments and simulation were measured at the sample corners.

6.4 Result Comparison. The downward bending of samples appeared in both experiment and simulation after one curing cycle, which is primarily due to different cooling rates on bottom and top surfaces of the samples, and stress relaxation of the resin. Three samples have been tested. For demonstration, Figs. 22(*a*) and 22(*b*) show post-curing deflection on the top surface of one sample predicted by the numerical model and measured by the DIC, respectively. It can be observed that the deflection contour from the simulation and experiment exhibits good consistency.

The high temperature gradient and its result of nonuniform DOC distribution within the sample were designed intentionally to introduce significant curing-induced deformation for clearer measurement and validation. Although the fast heating at around 9 °C will lead to high temperature gradient and nonuniform DOC distribution, it does not affect the validation of the developed models as DOC evolution within the sample could be precisely captured in the simulation using the established curing kinetic and heat transfer models.

The maximum deflection on the top surface of the sample from experimental DIC measurement and simulation is listed in Table 7 for comparison. The established resin curing model is capable of capturing post-curing deflection with less than 7% average error, making it suitable for industry application or to serve as a foundation for more complicated CFRP composite resin curing modeling. In the fabrication of partially cured samples, especially the ones with large thickness, it is difficult to achieve perfectly uniform curing status throughout the samples due to exothermic reaction and thermal gradient as mentioned in Sec. 5.1. However, it is extremely difficult to acquire actual DOC distribution within the entire samples, because the DSC measurement of DOC requires the tested materials to be smashed. Therefore, for each sample, only average DOC could be obtained and was input to simulation, possibly introducing some errors in prediction results.

7 Conclusion

In this study, a numerical model was developed to simulate the curing process of the YZ-05 prepreg thermoset resin. Essential properties to be input to the model were experimentally characterized. Due to the high viscosity of the YZ-05 resin, a special degassing method was introduced utilizing vacuum and high temperatures based on DSC results. Curing kinetics described using the autocatalytic model was determined with the isothermal scan of the DSC. Thermal properties, including mass density, specific heat capacity, and thermal conductivity, of resin samples with various DOCs were identified following ASTM standards. The combination of DIC and thermography techniques was applied for CTE and CSC measurement to avoid significant resin creep observed in the conventional contact measuring method. Afterward, the viscoelastic constitutive law of the resin in different curing states was characterized using the DMA, and a numerical method was used to determine the shift factors.

The developed numerical model, with the characterized properties, was implemented in Abaqus Standard to predict the vertical deflection of beam-shaped resin samples. The comparison of the simulation results with the experimental ones shows that the numerical model is capable of predicting curing-induced deformation of the YZ-05 resin with less than 7% error. Therefore, the model can be applied to predict and analyze the curing of more complex composite materials and structures with the same resin matrix in the future.

Acknowledgment

The work described in this paper was supported by grants from the Research Grants Council of the Hong Kong Special Administrative Region, China (Project No. CUHK 24208921), and Shun Hing

Downloaded from http://asmedigitalcollection.asme.org/manufacturingscience/article-pdf/144/8/081007/6846352/manu_144_8_081007.pdf by Southern University of Science & Technology user on 18 April 2022

Institute of Advanced Engineering of The10.13039/501100004853 Chinese University of Hong Kong (Project No. RNE-p2-20; Funder ID: 10.13039/501100004853).

Conflict of Interest

There are no conflicts of interest.

Data Availability Statement

The data sets generated and supporting the findings of this article are obtainable from the corresponding author upon reasonable request.

References

[1] Zhang, W., Bostanabad, R., Liang, B., Su, X., Zeng, D., Bessa, M. A., Wang, Y., Chen, W., and Cao, J., 2019, "A Numerical Bayesian-Calibrated Characterization Method for Multiscale Prepreg Preforming Simulations With Tension-Shear Coupling," Compos. Sci. Technol., **170**, pp. 15–24.

[2] Lim, Y. C., Chen, J., Jun, J., Leonard, D. N., Brady, M. P., Warren, C. D., and Feng, Z., 2020, "Mechanical and Corrosion Assessment of Friction Self-piercing Rivet Joint of Carbon Fiber-Reinforced Polymer and Magnesium Alloy AZ31B," ASME J. Manuf. Sci. Eng., **143**(3), p. 031006.

[3] Dai, J., Xi, S., and Li, D., 2019, "Numerical Analysis of Curing Residual Stress and Deformation in Thermosetting Composite Laminates With Comparison Between Different Constitutive Models," Materials (Basel), **12**(4), p. 572.

[4] Zhu, Q., 2001, *Dimensional Accuracy of Thermoset Polymer Composites: Process Simulation and Optimization*, ProQuest Dissertations Publishing, Ann Arbor, MI.

[5] Granado, L., Kempa, S., Bremmert, S., Gregoriades, L. J., Brüning, F., Anglaret, E., and Fréty, N., 2017, "Isothermal DSC Study of the Curing Kinetics of an Epoxy/Silica Composite for Microelectronics," J. Microelectron. Electron. Packag., **14**(2), pp. 45–50.

[6] Yeo, H., 2018, "Curing Kinetics of Liquid Crystalline 4, 4′-Diglycidyloxybiphenyl Epoxy Cured With 4, 4′-Diaminodiphenylsulfone," Polymer, **159**, pp. 6–11.

[7] Zhao, Y., and Drummer, D., 2019, "Influence of Filler Content and Filler Size on the Curing Kinetics of an Epoxy Resin," Polymers, **11**(11), p. 1797.

[8] Saad, M. T., Miller, S. G., and Marunda, T., 2014, "Thermal Characterization of IM7/8552-1 Carbon-Epoxy Composites," ASME 2014 International Mechanical Engineering Congress and Exposition, Montreal, Quebec, Canada, Nov. 14–20.

[9] Meira de Souza, L. G., da Silva, E. J., and Meira de Souza, L. G. V., 2020, "Obtaining and Characterizing a Polyester Resin and Cement Powder Composites," Mater. Res., **23**(5).

[10] Hu, H., Li, S., Wang, J., Zu, L., Cao, D., and Zhong, Y., 2017, "Monitoring the Gelation and Effective Chemical Shrinkage of Composite Curing Process With a Novel FBG Approach," Compos. Struct., **176**, pp. 187–194.

[11] Khoun, L., Centea, T., and Hubert, P., 2010, "Characterization Methodology of Thermoset Resins for the Processing of Composite Materials—Case Study: CYCOM 890RTM Epoxy Resin," J. Compos. Mater., **44**(11), pp. 1397–1415.

[12] Choi, S. H., and Yoon, S. H., 2019, "Prediction of Long-Term Viscoelastic Performance of PET Film Using RH-DMA," Compos. Res., **32**(6), pp. 382–387.

[13] Miller, T., Wojnar, C., and Louke, J., 2017, "Measuring Propellant Stress Relaxation Modulus Using Dynamic Mechanical Analyzer," J. Propul. Power, **33**(5), pp. 1252–1259.

[14] Ghosh, S. K., Rajesh, P., Srikavya, B., Rathore, D. K., Prusty, R. K., and Ray, B. C., 2018, "Creep Behaviour Prediction of Multi-layer Graphene Embedded Glass Fiber/Epoxy Composites Using Time–Temperature Superposition Principle," Composites, Part A, **107**, pp. 507–518.

[15] Nakada, M., and Miyano, Y., 2015, "Advanced Accelerated Testing Methodology for Long-Term Life Prediction of CFRP Laminates," J. Compos. Mater., **49**(2), pp. 163–175.

[16] Ahmed, J., 2017, "Time–Temperature Superposition Principle and Its Application to Biopolymer and Food Rheology," *Advances in Food Rheology and Its Applications*, J. Ahmed, P. Ptaszek, and S. Basu, eds., Woodhead Publishing, Cambridge, UK, pp. 209–241.

[17] Buttlar, W. G., Roque, R., and Reid, B., 1998, "Automated Procedure for Generation of Creep Compliance Master Curve for Asphalt Mixtures," Transp. Res. Rec., **1630**(1), pp. 28–36.

[18] Naya, S., Meneses, A., Tarrío-Saavedra, J., Artiaga, R., López-Beceiro, J., and Gracia-Fernández, C., 2013, "New Method for Estimating Shift Factors in Time–Temperature Superposition Models," J. Therm. Anal. Calorim., **113**(2), pp. 453–460.

[19] Liu, X., Luo, W., and Li, M., 2015, "A Novel Approach for Constructing Master Curves of Rheological Simple Material," Chin. J. Solid Mech., **36**(3), pp. 223–232.

[20] Skoczylas, J., Samborski, S., and Kłonica, M., 2021, "A Multilateral Study on the FRP Composite's Matrix Strength and Damage Growth Resistance," Compos. Struct., **263**, p. 113752.

[21] Kravchenko, O. G., Kravchenko, S. G., Casares, A., and Pipes, R. B., 2015, "Digital Image Correlation Measurement of Resin Chemical and Thermal Shrinkage After Gelation," J. Mater. Sci., **50**(15), pp. 5244–5252.

[22] Puentes, J., Restrepo-Zapata, N. C., Chaloupka, A., Duddleston, L. J. L., Rudolph, N., and Osswald, T. A., 2017, "Quasi-Isothermal DSC Testing of Epoxy Adhesives Using Initial Fast Heating Rates," J. Appl. Polym. Sci., **134**(42), p. 45425.

[23] Ren, R., Xiong, X., Ma, X., Liu, S., Wang, J., Chen, P., and Zeng, Y., 2016, "Isothermal Curing Kinetics and Mechanism of DGEBA Epoxy Resin With Phthalide-Containing Aromatic Diamine," Thermochim. Acta, **623**, pp. 15–21.

[24] Ryu, S. H., Sin, J. H., and Shanmugharaj, A. M., 2014, "Study on the Effect of Hexamethylene Diamine Functionalized Graphene Oxide on the Curing Kinetics of Epoxy Nanocomposites," Eur. Polym. J., **52**, pp. 88–97.

[25] Gómez-Jimenez, S., Becerra-Ferreiro, A., Jareño-Betancourt, E., and Vázquez-Penagos, J., 2021, "Phenomenological Analysis of the Cured Kinetics in the Order n of the Reaction As a Function of the Temperature of an EPDM Polymer," ASME J. Manuf. Sci. Eng., **143**(8), p. 081011.

[26] Kenny, J. M., 1994, "Determination of Autocatalytic Kinetic Model Parameters Describing Thermoset Cure," J. Appl. Polym. Sci., **51**(4), pp. 761–764.

[27] ASTM D792-20, 2020, *Standard Test Methods for Density and Specific Gravity (Relative Density) of Plastics by Displacement*, ASTM International, West Conshohocken, PA

[28] ASTM E1269-11, 2018, *Standard Test Method for Determining Specific Heat Capacity by Differential Scanning Calorimetry*, ASTM International, West Conshohocken, PA

[29] Fesko, D. G., and Tschoegl, N. W., 1971, "Time–Temperature Superposition in Thermorheologically Complex Materials," J. Polym. Sci., Part C: Polym. Symp., **35**(1), pp. 51–69.

[30] Kim, Y. K., and White, S. R., 1996, "Stress Relaxation Behavior of 3501-6 Epoxy Resin During Cure," Polym. Eng. Sci., **36**(23), pp. 2852–2862.

[31] ASTM E1461-13, 2013, *Standard Test Method for Thermal Diffusivity by the Flash Method*, ASTM International, West Conshohocken, PA

[32] Zhang, J. T., Zhang, M., Li, S. X., Pavier, M. J., and Smith, D. J., 2016, "Residual Stresses Created During Curing of a Polymer Matrix Composite Using a Viscoelastic Model," Compos. Sci. Technol., **130**, pp. 20–27.

[33] Ahn, H., Park, T., Li, Y., Yeo, S. Y., and Pourboghrat, F., 2021, "Mechanical Analysis of a Thermo-Hydroforming Fiber-Reinforced Composite Using a Preferred Fiber Orientation Model and Considering Viscoelastic Properties," ASME J. Manuf. Sci. Eng., **144**(2), p. 021008.

[34] ASTM D7028-07, 2015, *Standard Test Method for Glass Transition Temperature (DMA Tg) of Polymer Matrix Composites by Dynamic Mechanical Analysis (DMA)*, ASTM International, West Conshohocken, PA

[35] ASTM E1545-11, 2016, *Standard Test Method for Assignment of the Glass Transition Temperature by Thermomechanical Analysis*, ASTM International, West Conshohocken, PA

[36] Zarrelli, M., Skordos, A. A., and Partridge, I. K., 2002, "Investigation of Cure Induced Shrinkage in Unreinforced Epoxy Resin," Plast. Rubber Compos., **31**(9), pp. 377–384.

[37] O'Brien, D. J., Mather, P. T., and White, S. R., 2001, "Viscoelastic Properties of an Epoxy Resin During Cure," J. Compos. Mater., **35**(10), pp. 883–904.

[38] Ruiz, E., and Trochu, F., 2005, "Thermomechanical Properties During Cure of Glass-Polyester RTM Composites: Elastic and Viscoelastic Modeling," J. Compos. Mater., **39**(10), pp. 881–916.

[39] ASTM D638-14, 2014, *Standard Test Method for Tensile Properties of Plastics*, ASTM International, West Conshohocken, PA.

[40] Bogetti, T. A., and Gillespie, J. W., Jr., 1992, "Process-Induced Stress and Deformation in Thick-Section Thermoset Composite Laminates," J. Compos. Mater., **26**(5), pp. 626–660.

Downloaded from http://asmedigitalcollection.asme.org/manufacturingscience/article-pdf/144/8/081007/6846352/manu_144_8_081007.pdf by Southern University of Science & Technology user on 18 April 2022